Journal of the European Ceramic Society xxx (xxxx) xxx–xxx

Contents lists available at ScienceDirect

Journal of the European Ceramic Society

journal homepage: www.elsevier.com/locate/jeurceramsoc

Original Article

Low temperature thermoelectric properties of K-substituted $Bi_2Sr_2Co_2O_y$ ceramics prepared via laser floating zone technique

B. Özçelik[a,*], G. Çetin[a], M. Gürsul[a], M.A. Madre[b], A. Sotelo[b], S. Adachi[c], Y. Takano[c]

[a] Department of Physics, Faculty of Sciences and Letters, Çukurova University, 01330, Adana, Turkey
[b] ICMA (CSIC-Universidad de Zaragoza), C/María de Luna 3, 50018, Zaragoza, Spain
[c] National Institute for Materials Science, 1-2-1 Sengen, Tsukuba, Ibaraki, 305-0047, Japan

ARTICLE INFO

Keywords:
Thermoelectric oxides
Texture
Microstructure
Electrical properties
Figure of Merit

ABSTRACT

In the present study, $Bi_2Sr_{2-x}K_xCo_2O_y$ (x = 0.0, 0.050, 0.075, 0.100, and 0.15) ceramic precursors have been produced using the classical ceramic route, followed by texturing through the laser floating zone technique. XRD results show that the thermoelectric phase is the major one in all cases. Moreover, K-substitution decreases the secondary phases content, when compared to the undoped sample. SEM observations indicate that grain orientation is significantly enhanced when K-content is increased. K-doping decreases electrical resistivity from 32 10^{-5} Ω m (in undoped samples) to 20–22 10^{-5} Ω m at 300 K, while increasing Seebeck coefficient from 55 μV/K to 100–117 μV/K at 300 K. On the other hand, thermal conductivity is slightly lower in undoped samples (0.93 W/K m, compared to 1.10–1.28 W/K m for doped ones at 300 K), due to their lower electrical conductivity. Finally, ZT values are higher when the K-content increases up to x = 0.10, reaching 0.029 at around 400 K, and slightly decreasing for higher doping levels.

1. Introduction

Thermoelectric energy conversion can be used to transform thermal energy to electrical energy directly owing to the well-known Seebeck effect [1–3]. This physical phenomenon permits producing electrical energy from a thermal gradient between the cold and the hot side of a thermoelectric system. The conversion efficiency of such materials is usually characterized by the dimensionless thermoelectric figure of merit, ZT, defined as $TS^2/\rho\kappa$, where S is the Seebeck coefficient, ρ the electrical resistivity, κ the thermal conductivity, and T, the absolute temperature [4]. In general, high ZT materials require high S, low ρ, low κ, and high working temperature. Since the discovery of large thermoelectric properties in $NaCo_2O_4$ [5], and other Co-based materials [6–10], these layered cobalt oxides have become an alternative to the classical TE materials like Bi_2Te_3, PbTe, Sb_2Te_3, etc [11–13]. These oxide TE materials are neither toxic nor harmful to the environment, and the raw materials are inexpensive. Their chemical and thermal stability allows them operating at high temperatures under air without degradation. On the other hand, they still show relatively low thermoelectric performances and, consequently, it is assumed that developing thermoelectric (TE) materials with high efficiency is necessary for using them in electric power generation.

The crystal structure of these cobalt oxides can be described through a monoclinic system composed, in turn, by two different layers alternatively stacked. They are a common conductive CoO_2 layer with CdI_2-type structure, and an insulating block with rock-salt type structure. Both sublattices have common a- and c-axis lattice parameters and β angles but different b-axis length, producing a misfit along the b-direction [14,15]. The high anisotropy of this crystal structure is reflected in a large electrical anisotropy, opening the possibility to tune up electrical conductivity through grain alignment. Moreover, modifications of misfit factor, and/or oxidation states of cations in the rock-salt substructure have been also shown to influence electrical resistivity and Seebeck coefficient [16]. Furthermore, these modifications can be performed through relatively simple procedures, as cation substitution [17–23], or using different texturing techniques [22,24–28]. Among them, the Laser Floating Zone (LFZ) technique [29] offers some advantages, compared to other processes, as high density, large grain sizes and good grain orientation, together with a relatively high growth rate.

$Bi_2Sr_2CaCu_2O_y$ and $Bi_2Sr_2Co_2O_x$ materials are very similar from the point of view of their melting behavior. Consequently, taking into account the effect of Na- and K- substitution in the former one [30,31], previous works studied the effect of Na- or K- substitution on the high temperature thermoelectric properties of $Bi_2Sr_2Co_2O_y$ materials [18,20,22]. In this work, emphasis is put on the investigation on the effect of K aliovalent substitution for Sr on the microstructure, and low

* Corresponding author.
E-mail address: ozcelik@cu.edu.tr (B. Özçelik).

https://doi.org/10.1016/j.jeurceramsoc.2019.04.029
Received 18 January 2019; Received in revised form 10 April 2019; Accepted 12 April 2019

temperature thermoelectric performances of laser floating zone (LFZ) textured $Bi_2Sr_2Co_2O_y$ materials.

2. Experimental

Polycrystalline $Bi_2Sr_{2-x}K_xCo_2O_y$ precursors (x = 0, 0.05, 0.075, 0.10, and 0.15) were produced by the conventional solid state reaction using appropriate amounts of Bi_2O_3 (99%, Panreac), $SrCO_3$ (99%, Panreac), K_2CO_3 (99%, Panreac), and CoO (99.99%, Aldrich). They were mixed and ball milled 30 min at 300 rpm with distilled water, which was evaporated from the slurries using infrared lamps. After drying, the resulting powders were manually milled and subjected to two step calcination procedure for 12 h at 750 and 800 °C, in order to eliminate CO_2 from the metallic carbonates. These steps will avoid the release of CO_2 in the melting process, which would cause instabilities in the solidification interface [32]. Calcined powders were then isostatically pressed at ~200 MPa to produce cylindrical rods (φ = 2–3 mm, and length ~ 100 mm) which were directionally grown using Nd:YAG laser radiation (λ = 1064 nm) in a LFZ system [33]. Growth conditions were fixed at 30 mm/h for all samples. Moreover, during the growth process, the seed rotates at 3 rpm to keep the cylindrical geometry, while the feed was rotated in the opposite direction at 15 rpm to homogenize the molten zone. In these conditions, the textured bars have a constant diameter of around 2.5 mm. On the other hand, they show the presence of several secondary phases due to their incongruent melting [34,35]. Consequently, it is necessary to perform an annealing process (24 h at 810 °C, followed by furnace cooling to room temperature) to form the TE phase.

The phases identification has been done on powdered samples by X-ray diffraction (XRD) from 5 to 70° in a Rigaku D/max-B system. The evolution of microstructure with K-content was performed on longitudinal polished sections of samples in a field emission scanning electron microscope (FESEM, Zeiss Merlin), with an attached EDS system. For these observations, samples were hot-embedded into conducting resin, grinded to reach the center of the fibers, and finally polished with diamond paste. Density of samples has also been determined through Archimedes method, taking 6.8 g/cm^3 as theoretical density [35]. ρ, κ and S have been simultaneously measured from 4.2–390 K in a Quantum Design PPMS system. Figure of Merit, ZT (= $S^2T/\rho\kappa$), was calculated to establish the electrical performances of these samples as a function of temperature and K-content.

3. Results and discussion

The powder XRD patterns of all samples are presented in Fig. 1. In spite of the different K-content, all patterns are very similar and show

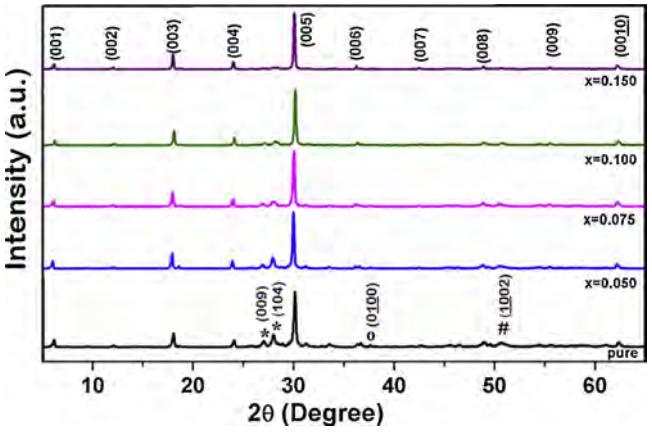

Fig. 1. Powder XRD patterns of $Bi_2Sr_{2-x}K_xCo_2O_y$ textured samples. The peaks of thermoelectric phase are shown by the diffraction planes. *, **o**, and # correspond to $Bi_{0.75}Sr_{0.25}O_y$, $CoCo_2O_4$, and CoO secondary phases, respectively.

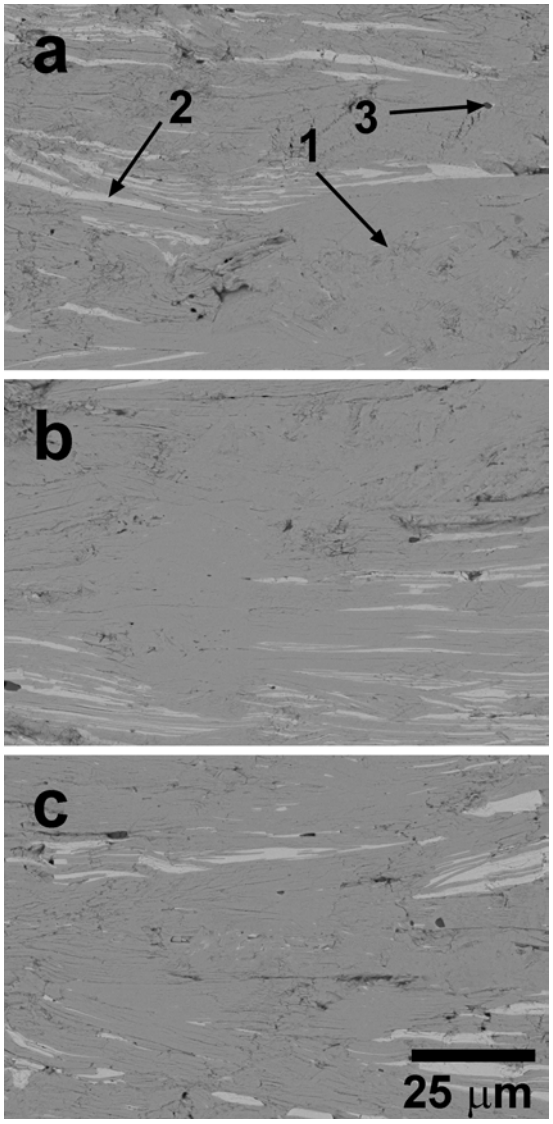

Fig. 2. Representative SEM micrographs of $Bi_2Sr_{2-x}K_xCo_2O_y$ textured samples, for x= ***(a)*** x = 0; ***(b)*** 0.075; and ***(c)*** 0.15.

that the highest peaks (indicated by their diffraction planes) correspond to the TE phase [36,37], appearing as the major one in all cases. In addition, these peaks correspond to its *ab*-planes [38], which can be explained by the large surface of grains in these planes, leading to their preferential orientation in the samples preparation process. Furthermore, undoped samples present several secondary phases, identified from the peaks identified by *($Bi_{0.75}Sr_{0.25}O_y$ [39]), **o**(Sr-rich Bi-Sr-Co-O [40]), and #(CoO_2 [41]). The intensity of these peaks decreases when K-doping is higher, pointing out to a decrease of secondary phases content induced by K.

Fig. 2 presents representative SEM images of longitudinal sections of samples. In these micrographs, it can be observed that all samples present three different contrasts. Grey contrast (#1) is the major one and has been associated, through EDS, to the $Bi_2Sr_{2-x}K_xCo_2O_y$ thermoelectric phase. White and dark grey contrasts correspond to $Bi_{0.75}Sr_{0.25}O_y$ (#2) and Sr-rich Bi-Sr-Co-O (#3) secondary phases, respectively, in minor amounts. Furthermore, the typical very low porosity produced in materials processed by LFZ [36], can also be seen in these micrographs. It has been confirmed by density measurements, which were around 97.3 ± 1.5% of the theoretical one in all samples, in agreement with previous works [22]. On the other hand, K-doping increases the grain alignment (compared to the undoped samples) up to

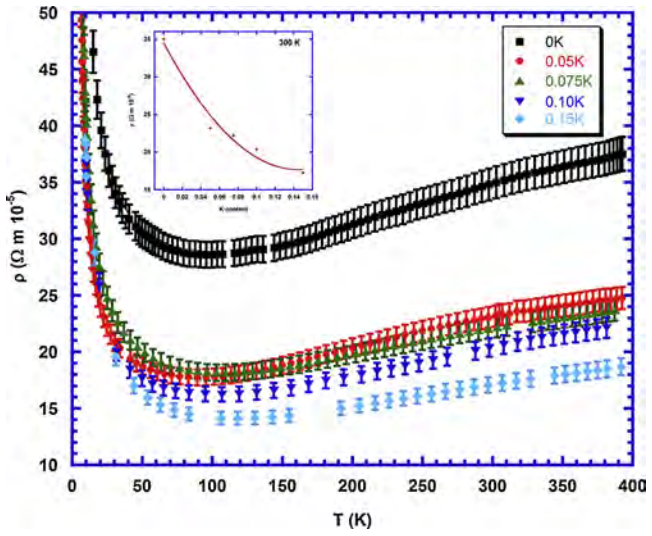

Fig. 3. Temperature dependence of electrical resistivity for all samples. The insert in the panel shows the room temperature resistivity.

0.10, slightly decreasing for further K-content. This behavior is due to the decrease of melting point of samples induced by K_2CO_3, which is reflected in a better grain alignment provided by a lower radial gradient in the solidification front, as observed in similar systems [42].

The temperature dependence of resistivity, $\rho(T)$, has been determined under zero magnetic field between 4.2 and 400 K, and the results are presented in Fig. 3, together with their 4% uncertainty, in agreement with previous works [43,44]. The measurements show semiconducting behavior ($d\rho/dT < 0$) for all samples in the low temperature range. When the temperature increases, a broad minimum around *Tmin*, defined as the metal-insulator-transition-temperature (MIT), appears in the resistivity curve, pointing out the existence of incommensurate spin-density-wave (IC-SDW) ordering [45]. From this temperature, the samples exhibit metallic behavior ($d\rho/dT > 0$) up to so-called T^* temperature, identifying the transition from a strongly correlated Fermi liquid regime to incoherent metal regime [46]. *Tmin*, T^* and room temperature resistivity values are displayed in Table 1. As it can be seen in the inset of Fig. 3, room temperature resistivity values monotonically decrease when K-content increases, while *Tmin* and T^* values increase up to 0.10 K-substitution. This resistivity evolution can be explained by the reduction of the oxidation state in the rock salt layer provided by the substitution of Sr^{2+} by K^+. Consequently, in order to keep electrical neutrality of the structure, some Co^{3+} is promoted to Co^{4+}, increasing the charge carrier concentration and decreasing resistivity. The minimum values at room temperature ($20*10^{-5}$ Ω m) have been obtained in 0.10 K-doped samples, which are higher than the obtained in sintered or hot-pressed materials (18, and $9*10^{-5}$ Ω m, respectively) [47], but lower than the measured in LFZ grown samples at 30 mm/h ($25*10^{-5}$ Ω m) [48].

In order to deeply investigate the conduction mechanism at temperatures below 37 K, the variable-range hopping (VRH) model [28] has been used. According to this model, the relation between resistivity and temperature can be defined as

$$\rho(T) = \rho(0)\ exp\ (T_0/T)^{1/3} \quad (1)$$

where $\rho(0)$ is a constant and $T_0 = 8/[\pi k_B N(\varepsilon_F) l_\nu^2]$ is the VRH characteristic temperature associated to the density of localized states at Fermi level $N(\varepsilon F)$, with l_ν as the localization length and k_B as the Boltzmann constant [49]. This model provides the best fitting of resistivity curves, as shown in Fig. 4a, where the linearity between $\ln\rho(T)$ and $T^{-1/3}$ points out that all data below 37 K are well-fitted. The obtained fitting parameter T_0 values are also given in Table 1.

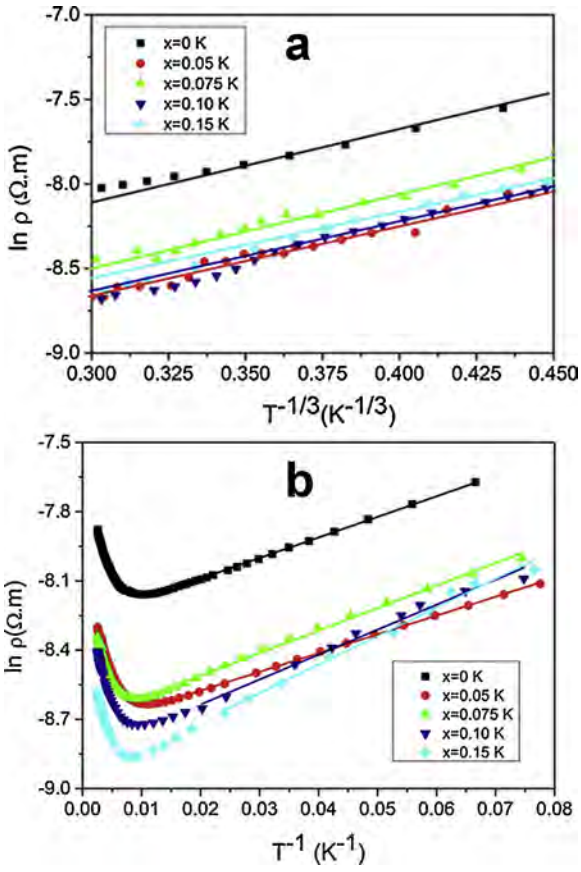

Fig. 4. Plots of (a) lnρ versus $T^{-1/3}$ between 10 and 37 K with the fitted lines for the samples of Fig. 3; and (b) lnρ versus T^{-1} between 12 and 380 K with the fitted lines for all reported samples.

According to thermally activated conduction (TAC) model [46,49], at temperatures above 37 K, the variation of resistivity with respect to temperature can be described as

$$\frac{1}{\rho} = \mu(T)\exp(-\frac{E_0}{k_B T}) \quad (2)$$

This formula can be organized as

$$ln\rho = \frac{E_0}{k_B}T^{-1} - ln\mu = AT^{-1} + B \quad (3)$$

Table 1
Electrical and thermal transport parameters for $Bi_2Sr_{2-x}K_xCo_2O_y$ textured samples with x = 0.0, 0.050, 0.075, 0.100, and 0.15.

Sample	x = 0.00	x = 0.05 K	x = 0.075 K	x = 0.10 K	x = 0.15 K
T_0 (K)	86 (∓0.1)	70 (∓0.2)	80 (∓0.2)	72 (∓0.3)	71 (∓0.3)
E_0 (meV)	0.77 (∓0.05)	0.71 (∓0.04)	0.84 (∓0.14)	0.93 (∓0.5)	1.06 (∓0.47)
T_{min}(K)	49 (∓1)	83 (∓1)	91 (∓2)	94 (∓2)	78 (∓2)
T^*	198 (∓3)	243 (∓3)	250 (∓3)	297 (∓3)	256 (∓3)
κ_{ch300K} ($WK^{-1}m^{-1}$)	0.02 (∓0.001)	0.03 (∓0.002)	0.03 (∓0.003)	0.04 (∓0.004)	0.04 (∓0.002)
ρ_{300K} (mΩ cm)	35.1 (∓0.07)	23.2 (∓0.02)	22.2 (∓0.01)	20.4 (∓0.02)	17.3 (∓0.01)

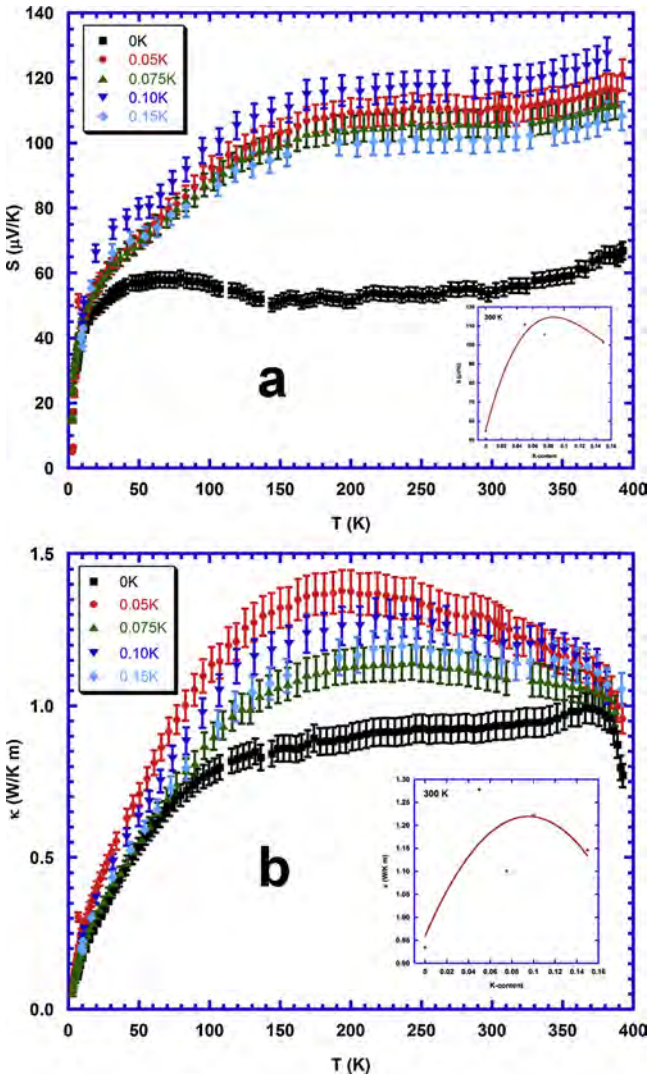

Fig. 5. (a) Temperature dependence of Seebeck coefficient of all reported samples. The insert shows the evolution of room temperature Seebeck coefficient; and (b) Temperature dependence of thermal conductivity $\kappa(T)$ samples. The insert shows the evolution of room temperature thermal conductivity.

where μ is the carrier mobility, E_0 is the energy gap arising from the spin density wave (SDW) at the Fermi surface, and $A = E_0/k_B$ and $B = -\ln\mu$ are the fitting parameters. The data obtained by applying Eq. (3) are presented in Fig. 4b, together with their linear fitting. From the slope of these lines, the activation energies of samples have been calculated and the results are displayed in Table 1. As it can be seen in the table, they increase when K-content is raised, pointing out to a positive effect on the formation of spin density wave state when K substitutes Sr in the structure.

The Seebeck coefficient variation with temperature is given in Fig. 5a, for all samples together with their 4% uncertainty, in agreement with previous works [43,44]. It exhibits a positive sign in the whole measured temperature range, meaning that all samples have p-type conduction mechanism, mainly governed by holes. K-substitution increases to about two times the values obtained in undoped samples. Moreover, as it can be seen in the inset of Fig. 5a, the Seebeck coefficient is raised until 0.10 K-substitution, slightly decreasing for further K-content. The highest Seebeck coefficient is observed at room temperature (117 μV/K), which is very close to that obtained in sintered materials under oxygen atmosphere (125 μV/K) [50], single crystals (115 μV/K) [51], or sinter-forged materials (110 μV/K) [19]. On the other hand, it is lower than the obtained in undoped LFZ as-grown samples at the same rate (135 μV/K) [48]. These differences can be explained by the different oxygen content in these samples, in agreement with Koshibae's equation [52].

Fig. 5b illustrates the temperature dependence of thermal conductivity, and its 5% uncertainty [43,44], for all samples. As it can be observed in the graph, all of them show very similar behavior in the whole measured temperature range. On the other hand, K-doped samples present higher thermal conductivity than the undoped one, in agreement with their lower electrical resistivity. However, the variations of thermal conductivity with changing K-content are not monotonic, the highest values are found for the 0.05 K-doped samples (see inset of Fig. 5b), probably due to two opposite contributions, as K-substitution i) increases hole carrier concentration, and ii) has larger ionic radius than Sr, and forms point defects which can widen the phonon scattering spectrum. In general, thermal conductivity is defined as the sum of the phonon thermal conductivity component κ_{ph}, and the carrier thermal conductivity component κ_{ch} [53]

$$\kappa = \kappa_{\mathrm{ph}} + \kappa_{\mathrm{ch}} \tag{4}$$

where the value of the κ_{ch} can be deduced based on the Wiedemann – Franz law, which relates κ_{ch} to ρ as $\kappa_{ch} = LT/\rho$, where L is the Lorentz number ($2.45 \times 10^{-8}\ \mathrm{V^2\,K^{-2}}$ for free electrons). Calculated κ_{ch} values are presented in Table 1. As it can be seen in the table, room temperature κ_{ch} values of K-substituted samples are slightly higher than those of the undoped ones. In this regard, this can be attributed to the distortion of crystal structure due to the size difference between K and Sr, strongly influencing the lattice vibrations in K-substituted samples. The lowest thermal conductivity values at room temperature (1.0 W/K m) are in the range of the best reported in the literature (0.60–2.81 W/K m) [54–56].

The thermoelectric performances were evaluated through ZT and presented, as a function of temperature, in Fig. 6, together with its 16% uncertainty [43,44]. In the graph, it can be seen that ZT increases when temperature is raised, in all cases. Moreover, all doped samples present much higher values than the undoped ones. On the other hand, K-content slightly modifies the ZT values, which are increased for higher K-doping up to 0.10, decreasing for further content. As can be seen from the inset in Fig. 6, the highest ZT values obtained in this work at room temperature (0.018) are in the order of those obtained in spark plasma textured materials or sintered from sol-gel prepared precursors (0.017 – 0.025) [54,55], but much higher than the obtained by melt quenching (0.010) [56].

All these data show that the LFZ texturing process, together with K-

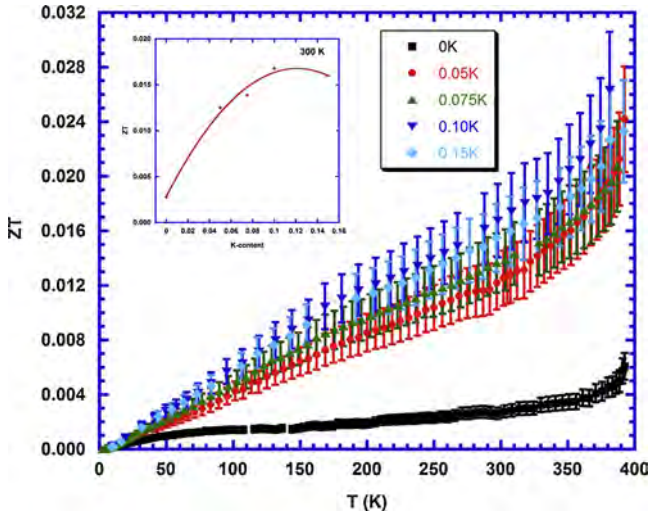

Fig. 6. Temperature dependence of dimensionless Figure of merit (ZT) of all samples reported in this study. The insert in the panel shows the evolution of room temperature figure of merit with K-content.

substitution is very competitive to produce high-performances textured thermoelectric materials.

4. Conclusion

In this research $Bi_2Sr_{2-x}K_xCo_2O_y$ textured samples with x = 0.0, 0.050, 0.075, 0.100, and 0.15 have been fabricated via LFZ. After annealing, XRD results have shown that the major phase is the thermoelectric one, and K-substitution decreases the amount of secondary phases observed. SEM observations showed that grain orientation is enhanced with K-content. Moreover, K-doping leads to a decrease of room temperature resistivity from 32 10^{-5} Ω m (in undoped samples) to 20–22 10^{-5} Ω m. A broad minimum around the metal-insulator-temperature (MIT) labeled as *Tmin* was observed in the resistivity curve, attributed to the existence of incommensurate spin-density-wave ordering. Seebeck coefficient of all K-substituted samples was almost two times larger than for the undoped one, reaching 117 μV/K in 0.10 K-doped samples. Thermal conductivities of K-substituted samples were larger than in the undoped one (1.10–1.28 W/K m compared to 0.93 W/K m, at 300 K). Finally, ZT values increased with the K-content up to 0.10, reaching 0.029 at around 400 K, decreasing for higher K-doping.

Acknowledgements

This work is supported by Research Fund of Çukurova University, Adana, Turkey, under grant contracts no: FDK-2016-6105 and FBI-2017-9225. M. A. Madre and A. Sotelo wish to thank the Gobierno de Aragón-FEDER (Research Group T 54-17 R), and the Spanish MINECO-FEDER (MAT2017-82183-C3-1-R) for financial support. The use of Servicio General de Apoyo a la Investigación-SAI, Universidad de Zaragoza is also acknowledged.

References

[1] G. Mahan, B. Sales, J. Sharp, Thermoelectric materials: new approaches to an old problem, Phys. Today 50 (1997) 42–47.
[2] L.E. Bell, Cooling, heating, generating power, and recovering waste heat with thermoelectric systems, Science 32 (2008) 1457.
[3] M.H. Elsheikh, D.A. Shnawah, M.F.M. Sabri, S.B.M. Said, M.H. Hassan, M.B.A. Bashir, M. Mohamad, A review on thermoelectric renewable energy: principle parameters that affect their performance, Renew. Sust. Energy Rev. 30 (2014) 337.
[4] D.M. Rowe, Thermoelectrics Handbook: Macro to Nano, 1st ed., CRC Press, Boca Raton, FL, 2006.
[5] I. Terasaki, Y. Sasago, K. Uchinokura, Large thermoelectric power in $NaCo_2O_4$ single crystals, Phys. Rev. B 56 (1997) R12685.
[6] A.C. Masset, C. Michel, A. Maignan, M. Hervieu, O. Toulemonde, F. Studer, B. Raveau, J. Hejtmanek, Misfit-layered cobaltite with an anisotropic giant magnetoresistance: $Ca_3Co_4O_9$, Phys. Rev. B 62 (2000) 166.
[7] R. Funahashi, M. Shikano, $Bi_2Sr_2Co_2O_y$, whiskers with high thermoelectric figure of merit, Appl. Phys. Lett. 81 (2002) 1459.
[8] A. Sotelo, E. Guilmeau, S.h. Rasekh, M.A. Madre, S. Marinel, J.C. Diez, Enhancement of the thermoelectric properties of directionally grown Bi–Ca–Co–O through Pb for Bi substitution, J. Eur. Ceram. Soc. 30 (2010) 1815.
[9] S. Hébert, S. Lambert, D. Pelloquin, A. Maignan, Large thermopower in a metallic cobaltite: the layered Tl-Sr-Co-O misfit, Phys. Rev. B 64 (2001) 172101.
[10] R. Funahashi, I. Matsubara, S. Sodeoka, Thermoelectric properties of $Bi_2Sr_2Co_2O_x$ polycrystalline materials, Appl. Phys. Lett. 76 (2000) 2385.
[11] J.M. Santamaria, J. Alkorta, J.G. Sevillano, Mechanical properties of bismuth telluride (Bi_2Te_3) processed by high pressure torsion (HPT), Bol. Soc. Esp. Ceram. V. 52 (2013) 137.
[12] H.C. Wang, J.-H. Bahk, C. Kang, J. Hwang, K. Kim, J. Kim, P. Burke, J.E. Bowers, A.C. Gossard, A. Shakouri, W. Kim, Right sizes of nano- and microstructures for high-performance and rigid bulk thermoelectrics, Proc. Natl. Acad. Sci. U. S. A. 111 (2014) 10949.
[13] H.C. Wang, J. Hwang, M.L. Snedaker, I.-H. Kim, C. Kang, J. Kim, G.D. Stucky, J. Bowers, W. Kim, High thermoelectric performance of a heterogeneous PbTe nanocomposite, Chem. Mater. 27 (2015) 944.
[14] Y. Miyazaki, Crystal structure and thermoelectric properties of the misfit-layered cobalt oxides, Solid State Ion. 172 (2004) 463.
[15] H. Leligny, D. Grebille, O. Perez, A.C. Masset, M. Hervieu, B. Raveau, A five-dimensional structural investigation of the misfit layer compound $[Bi_{0.87}SrO_2]_2[CoO_2]_{1.82}$, Acta Cryst. B 56 (2000) 173.
[16] A. Maignan, D. Pelloquin, S. Hebert, Y. Klein, M. Hervieu, Thermoelectric power in misfit cobaltites ceramics: Optimization by chemical substitutions, Bol. Soc. Esp. Ceram. V. 45 (2006) 122.
[17] H.S. Hao, Q.L. He, L.M. Zhao, Thermoelectric properties of Cu-substituted $Bi_2Ca_2Co_2O_y$ misfit oxides, Adv. Mater. Res. 284-286 (2011) 2263.
[18] G. Çetin Karakaya, B. Özçelik, O. Nane, A. Sotelo, S.h. Rasekh, M.A. Torres, M.A. Madre, Improvement of $Bi_2Sr_2Co_2O_y$ thermoelectric performances by Na doping, J. Electroceram. 40 (2018) 11.
[19] W. Shin, N. Murayama, Thermoelectric properties of (Bi, Pb)–Sr–Co–O oxide, J. Mater. Res. 15 (2000) 382.
[20] G. Çetin Karakaya, B. Özçelik, M.A. Torres, M.A. Madre, A. Sotelo, Effects of K substitution on thermoelectric and magnetic properties of $Bi_2Sr_2Co_2O_y$ ceramic, J. Mater. Sci. Mater. Electron. 28 (2017) 12652.
[21] H.Q. Liu, X.B. Zhao, T.J. Zhu, Y. Song, F.P. Wang, Thermoelectric properties of Gd, Y co-doped $Ca_3Co_4O_{9+\delta}$, Curr. Appl. Phys. 9 (2009) 409.
[22] G. Çetin Karakaya, B. Özçelik, M.A. Torres, M.A. Madre, A. Sotelo, Effect of Na-doping on thermoelectric and magnetic performances of textured $Bi_2Sr_2Co_2O_y$ ceramics, J. Eur. Ceram. Soc. 38 (2018) 515.
[23] Y. Tanaka, T. Fujii, M. Nakanishi, Y. Kusano, H. Hashimoto, Y. Ikeda, J. Takada, Systematic study on synthesis and structural, electrical transport and magnetic properties of Pb-substituted Bi–Ca–Co–O misfit-layer cobaltites, Solid State Commun. 141 (2007) 122.
[24] S.h. Rasekh, G. Constantinescu, M.A. Torres, M.A. Madre, J.C. Diez, A. Sotelo, Growth rate effect on microstructure and thermoelectric properties of melt grown $Bi_2Ba_2Co_2O_x$ textured ceramics, Adv. Appl. Ceram. 111 (2012) 490.
[25] Y. Zhang, J. Zhang, Q. Lu, Synthesis of highly textured $Ca_3Co_4O_9$ ceramics by spark plasma sintering, Ceram. Int. 33 (2007) 1305.
[26] S.h. Rasekh, M.A. Madre, J.C. Diez, E. Guilmeau, S. Marinel, A. Sotelo, Effect of Pb substitution on the thermoelectrical properties of textured $Bi_2Ca_2Co_{1.7}O_y$ ceramics prepared by a polymer solution method, Bol. Soc. Esp. Ceram. V. 49 (2010) 371.
[27] J.G. Noudem, D. Kenfaui, D. Chateigner, M. Granular Gomina, Lamellar thermoelectric oxides consolidated by spark plasma sintering, J. Korean Inst. Electr. Electron. Mater. Eng. 40 (2011) 1100.
[28] H. Itahara, C. Xia, J. Sugiyama, T. Tani, Fabrication of textured thermoelectric layered cobaltites with various rock salt-type layers by using β-$Co(OH)_2$ platelets as reactive templates, J. Mater. Chem. 14 (2004) 61.
[29] G.F. de la Fuente, J.C. Diez, L.A. Angurel, J.I. Peña, A. Sotelo, R. Navarro, Wavelength Dependence in Laser Floating-Zone Processing - A Case-Study with Bi-Sr-Ca-Cu-O Superconductors, Adv. Mater. 7 (1995) 853.
[30] O. Nane, B. Ozcelik, H. Amaveda, A. Sotelo, M.A. Madre, Improvement of structural and superconducting properties of Bi-2212 textured rods by substituting sodium, Ceram. Int. 42 (2016) 8473.
[31] B. Ozcelik, M. Gursul, A. Sotelo, M.A. Madre, Effect of K substitution on structural, electrical and magnetic properties of Bi-2212 system, J. Mater. Sci. Mater. Electron. 25 (2014) 4476.
[32] A. Sotelo, S.h. Rasekh, M.A. Torres, P. Bosque, M.A. Madre, J.C. Diez, Improved thermoelectric performances in textured $Bi_{1.6}Pb_{0.4}Ba_2Co_2O_y$/Ag composites, Ceram. Int. 42 (2016) 18592.
[33] A. Sotelo, S.h. Rasekh, G. Constantinescu, M.A. Torres, M.A. Madre, J.C. Diez, Improvement of textured $Bi_{1.6}Pb_{0.4}Sr_2Co_{1.8}O_x$ thermoelectric performances by metallic Ag additions, Ceram. Int. 39 (2013) 1597.
[34] S.h. Rasekh, F.M. Costa, N.M. Ferreira, M.A. Torres, M.A. Madre, J.C. Diez, A. Sotelo, Use of laser technology to produce high thermoelectric performances in $Bi_2Sr_2Co_{1.8}O_x$, Mater. Design 75 (2015) 143.
[35] E. Combe, R. Funahashi, T. Barbier, F. Azough, R. Freer, Decreased thermal conductivity in $Bi_2Sr_2Co_2O_x$ bulk materials prepared by partial melting, J. Mater. Res. 31 (2016) 1296.
[36] A. Sotelo, M.A. Torres, G. Constantinescu, S.h. Rasekh, J.C. Diez, M.A. Madre, Effect of Ag addition on the mechanical and thermoelectric performances of annealed $Bi_2Sr_2Co_{1.8}O_x$ textured ceramics, J. Eur. Ceram. Soc. 32 (2012) 3745.
[37] G.J. Xu, R. Funahashi, M. Shikano, I. Matsubara, Y.Q. Zhou, Thermoelectric properties of $Bi_{2.2-x}Pb_xSr_2Co_2O_y$ system, J. Appl. Phys. 91 (2002) 4344.
[38] M.A. Madre, S.h. Rasekh, J.C. Diez, A. Sotelo, New solution method to produce high performance thermoelectric ceramics: a case study of Bi-Sr-Co-O, Mater. Lett. 64 (2010) 2566.
[39] D. Mercurio, J.C. Champarnaud-Mesjard, B. Frit, P. Conflant, J.C. Boivin, T. Vogt, Thermal evolution of the crystal-structure of the rhombohedral $Bi_{0.75}Sr_{0.25}O_{1.375}$ phase–a single-crystal neutron-diffraction study, J. Solid State Chem. 112 (1994) 1.
[40] D. Pelloquin, A.C. Masset, A. Maignan, C. Michel, M. Hervieu, B. Raveau, A new cobaltite with a tubular structure: $Bi_{3.7}Sr_{11.4}Co_8O_{28-d}$, the n = 2 member of the series $(Bi_2Sr_2CoO_6)_n(Sr_8Co_6O_{16-d})$, Chem. Mater. 11 (1999) 84.
[41] R.J. Makkonen, Crystallographic and magnetic properties of solid solutions of $CoCo_2O_4$ and $CoCr_2O_4$, Suomen Kemistilehti A 35 (1962) 230.
[42] F.M. Costa, N.M. Ferreira, S.h. Rasekh, A.J.S. Fernandes, M.A. Torres, M.A. Madre, J.C. Diez, A. Sotelo, Very large superconducting currents induced by growth tailoring, Cryst. Growth Des. 15 (2015) 2094.
[43] S. Populoh, M.H. Aguirre, O.C. Brunko, K. Galazka, Y. Lu, A. Weidenkaff, High figure of merit in (Ti,Zr,Hf)NiSn half-Heusler alloys, Scr. Mater. 66 (2012) 1073.
[44] A. Sotelo, F.M. Costa, N.M. Ferreira, A. Kovalevsky, M.C. Ferro, V.S. Amaral, J.S. Amaral, S.h. Rasekh, M.A. Torres, M.A. Madre, J.C. Diez, Tailoring $Ca_3Co_4O_9$ microstructure and performances using atransient liquid phase sintering additive, J. Eur. Ceram. Soc. 36 (2016) 1025.
[45] J. Sugiyama, H. Itahara, T. Tani, J.H. Brewer, E.J. Ansaldo, Magnetism of layered cobalt oxides investigated by muon spin rotation and relaxation, Phys. Rev. B 66 (2002) 134413.
[46] Y. Huang, B. Zhao, R. Ang, S. Lin, Z. Huang, S. Tan, Y. Liu, W. Song, Y. Sun, Enhanced thermoelectric performance and room-temperature spin-state transition of Co^{4+} ions in the $Ca_3Co_{4-x}Rh_xO_9$ system, J. Phys. Chem. C 117 (2013) 11459.

[47] E. Combe, R. Funahashi, T. Barbier, F. Azough, R. Freer, Decreased thermal conductivity in $Bi_2Sr_2Co_2O_x$ bulk materials prepared by partial melting, J. Mater. Res. 31 (2016) 1296.
[48] J.C. Diez, E. Guilmeau, M.A. Madre, S. Marinel, S. Lemonnier, A. Sotelo, Improvement of $Bi_2Sr_2Co_{1.8}O_x$ thermoelectric properties by laser floating zone texturing, Solid State Ion. 180 (2009) 827.
[49] N.F. Mott, E.A. Davis, Electronic Processes in Non-Crystalline Materials, Clarendon Press, London, 1971.
[50] J.L. Lan, Y.H. Lin, G.J. Li, S.L. Xu, Y. Liu, C.W. Nan, S. Zhao, High temperature electrical transport behaviors of the layered $Ca_2Co_2O_5$-based ceramics, Appl. Phys. Lett. 96 (2010) 192104.
[51] T. Itoh, I. Terasaki, Thermoelectric properties of $Bi_{2.3-x}Pb_xSr_{2.6}Co_2O_y$ single crystals, J. Appl. Phys. 39 (2000) 6658.
[52] W. Koshibae, K. Tsuitsui, S. Maekawa, Thermopower in cobalt oxides, Phys.Rev. B 62 (2000) 6869.
[53] Y. Wang, Y. Sui, X.J. Wang, W.H. Su, X.Y. Liu, Enhanced high temperature thermoelectric characteristics of transition metals doped $Ca_3Co_4O_{9+\delta}$ by cold high-pressure fabrication, J. Appl. Phys. 107 (2010) 033708.
[54] K. Rubesova, T. Hlasek, V. Jakes, S. Huber, J. Hejtmanek, D. Sedmidubsky, Effect of a powder compaction process on the thermoelectric properties of $Bi_2Sr_2Co_{1.8}O_x$ ceramics, J. Eur. Ceram. Soc. 35 (2015) 525.
[55] K. Rubesova, T. Hlasek, V. Jakes, D. Sedmidubsky, J. Hejtmanek, Water based sol–gel methods used for Bi-222 thermoelectrics preparation, J. Solgel Sci. Technol. 64 (2012) 93.
[56] J. Lingner, R. Funahashi, E. Combe, M. Letz, G. Jakob, Thermoelectric sintered glass-ceramics with a $Bi_2Sr_2Co_2O_x$ phase, Appl. Phys. A 120 (2015) 59.